Atomic and electronic structure of decagonal Al-Ni-Co alloys and approximant phases

M. Krajčí
Institut für Material Physik and Center for Computational Materials Science, Universität Wien, Sensengasse 8, A-1090 Wien, Austria and Institute of Physics, Slovak Academy of Sciences, SK-84228, Bratislava, Slovakia

J. Hafner
Institut für Material Physik and Center for Computational Materials Science, Universität Wien, Sensengasse 8, A-1090 Wien, Austria

M. Mihalkovič
Institute of Physics, Slovak Academy of Sciences, SK-84228, Bratislava, Slovakia and Institut für Physik, Technische Universität Chemnitz, D-09107 Germany

(Received 20 May 1999; revised manuscript received 16 March 2000)

Detailed investigations of the atomic and electronic structures of decagonal AlNiCo alloys have been performed. Several different models for the decagonal structure have been investigated: A model based on a rhombic-hexagon tiling proposed by Henley and models based on a cluster decoration of the Penrose tiling with large rhombus edge. The topology of the structural models has been refined on the basis of the existing x-ray-diffraction data which, however, do not allow us to specify the chemical decoration uniquely. The chemical order on the decagonal lattice has been optimized via the comparison of the calculated electronic spectra with photoemission and soft-x-ray data and using total-energy calculations. The electronic structure calculations for large periodic approximants with up to 1276 atoms/cell have been performed self-consistently using a real-space tight-binding linear muffin-tin orbital technique. The best agreement with the experimental spectra is achieved for a large-rhombus-tiling model with the innermost ring of the pentagonal columnar clusters occupied by Ni atoms only. This configuration also has the lowest total energy. As in decagonal AlCuCo we find a high density of states at the Fermi level, but the chemical ordering is very different: whereas in *d*-AlCuCo direct Cu-Cu neighbors are suppressed and there is a slight preference for Co-Co homocoordination, in *d*-AlNiCo a strong Ni-Ni interaction stabilizes the innermost Ni ring, direct Co-Co neighbors are suppressed and there is a strong Co-Al interaction.

I. INTRODUCTION

Soon after the discovery of icosahedral quasicrystals by Shechtman *et al.*,[1] a decagonal phase which is quasiperiodic in a plane perpendicular to the decagonal axis and periodic along that direction was identified in the Al-Mn system by Bendersky.[2] The decagonal Al-Mn quasicrystals were only metastable. Stable decagonal quasicrystals were discovered in the ternary AlCuCo and AlNiCo systems.[3,4] Due to the existence of samples of high structural quality, these two decagonal alloys have been widely investigated. Most studies are concerned with various structural aspects.[5–16] Originally it was believed that *d*-AlCuCo and *d*-AlNiCo quasicrystals are isotypic, but recent studies revealed the existence of a very complex phase diagram of the pseudobinary AlCo-AlNi system in the stability range of the decagonal phases, showing a large structural variety.[16–19] Ritsch *et al.*[16] report eight different structural modifications of decagonal phases. Most stable decagonal phases exist only at high temperatures in the range of 700–1100 K. The largest region of quasicrystalline stability exists at the composition close to $Al_{70}Ni_{15}Co_{15}$. The basic structures of *d*-AlCuCo and *d*-AlNiCo are, according to high-resolution electron microscopy (HREM), based on the same decagonal clusters with 20-Å diameter. However, whereas in *d*-AlCuCo the decagonal clusters do not overlap, in *d*-AlNiCo the existence of two distinct interatomic distances in the ratio $1:1/\tau$ leads to a partial overlap.[14] Several structural modifications of the *d*-AlNiCo phase have been identified.[5,6,10,16–28]

On the basis of the experimental information from diffraction studies, a number of structural models for *d*-Al-Co-Cu(Ni) alloys have been proposed. Steurer and Kuo[5] and Hiraga, Lincoln, and Sun[6] analyzed structure of the 20-Å decagonal cluster and proposed almost identical structural models of this cluster. However, this first model was not able to account for special features present in the superstructures of *d*-AlNiCo.[29] Burkov[20] proposed a model (here denoted as B1) based on a cluster decoration of the binary Penrose tiling with space-group symmetry $P10_5/mmc$. A second model (denoted as B2) by Burkov[21] is based on Klotz-triangle tiling (known also as Tübingen tiling) and matching rules enforcing quasiperiodicity. The matching rules are closely connected with the chemical order between Cu and Co atoms. The symmetry of this model is $P10_5/m$. Steurer *et al.*[10] also proposed a model based on columnar clusters similar to those found in monoclinic $Al_{13}Co_4$ such that the structure consists of flat and puckered layers. Six-layer stacks may be decomposed into slightly distorted triacontahedra with point-group symmetry 10 and space-group symmetry $P\overline{1}0m2$ for this model.[15] Hiraga, Sun, and Yamamoto[13] proposed a superstructure model having a 20-Å cluster on each vertex of a Penrose pattern with an edge length of 20 Å. Adjacent columnar clusters are related by a 10_5 screw axis. Yamamoto and co-workers[22,25] proposed later a corresponding five-dimensional superstructure model.

The electronic properties of decagonal alloys have been

widely investigated. As expected, electrical resistivity,[30–32] Hall effect,[33] thermopower,[30] thermal,[34] and optical conductivity[35] of *d*-AlCuCo and *d*-AlNiCo display a strong anisotropy, i.e., metallic behavior along and nonmetallic behavior perpendicular to the periodic axis. Both alloys are diamagnetic over a wide temperature range.[36] There have been many attempts to interpret the electronic properties by invoking a Hume-Rothery mechanism leading to the formation of a pseudogap at the Fermi level.[32,36] However, the existence of a pseudogap cannot be reconciled with the optical conductivity data[35] and with high-resolution photoemission spectroscopy[37–39] on both *d*-AlCuCo and *d*-AlNiCo. Soft x-ray spectroscopy[40] suggests the existence of a pseudogap in the partial Al-3*p* density of states (DOS), but does not exclude that in the total DOS this minimum is covered by a broad Cu-3*d* or Ni-3*d* band as suggested by the photoemission data. The photoemission and soft x-ray data also point to surprising differences in the electronic spectra of *d*-AlCuCo and *d*-AlNiCo. Whereas in *d*-$Al_{65}Cu_{20}Co_{15}$ the 3*d* bands of Cu and Co are split by 3 eV (the centers of gravity of the bands are located at binding energies of -3.7 and -0.7 eV), both bands overlap in *d*-$Al_{70}Ni_{15}Co_{15}$ and form a broad band centered at about -1.4-eV binding energy. The conclusions drawn from the resonant photoemission spectra are corrobated by the soft x-ray spectra. The difference in the spectra is too large to be explained solely by the different degree of band filling in Cu and Ni—evidently, the *d*-*d* interaction is fundamentally different in these two decagonal alloys.

Electronic structure calculations for *d*-AlCuCo based on zero-order approximants of the older Burkov model[20] (B1) consisting of a binary Penrose tiling with cluster decoration produce an unsplit *d*-band and a pseudogap at the Fermi level[42,43]—in evident disagreement with both photoelectron and soft x-ray spectra. Calculations based on the newer Burkov model[21] (model B2, Klotz-triangle tiling) agree with the measured spectra, but only if the decagonal acceptance domain for transition-metal (TM) atoms in the five-dimensional hyperspace is subdivided in such a way as to produce the correct chemical ordering between Co and Cu atoms.[43] The model producing the best agreement has no direct Cu-Cu neighbors at all, at a small Cu-Co coordination number ($N_{\text{Cu-Co}} \approx 2.3$). Co atoms have an increased coordination by transition metals, with slight preference for homocoordination ($N_{\text{Co-Cu}} \approx 2.4$, $N_{\text{Co-Co}} \approx 3.2$). This type of chemical ordering produces the most pronounced splitting between the *d* bands. It has also been pointed out that similar *d*-band shifts associated with short-range chemical ordering have been observed in amorphous TM alloys (both by experiment[44] and band-structure calculations[45,46]) and shown to play an essential role in the stabilization of these alloys.

The example of *d*-AlCuCo demonstrates that electronic structure calculations may be used to optimize the chemical order and even to eliminate certain structural models which lead to predictions for the electronic spectrum in contradiction with experiment, although they appear to be compatible with the diffraction and HREM data.

In the present work we apply a similar strategy to the more difficult case of *d*-AlNiCo. Our paper is arranged as follows: In Sec. II we briefly recapitulate some of the models that have been proposed and we motivate the choice of the small-rhombus-hexagon-tiling (SRHT) (Ref. 24) and the large-rhombus-tiling (LRT) (Refs. 5, 6, and 13) models for our study. In Sec. III we review very briefly the self-consistent tight-binding linear muffin-tin orbital (TB-LMTO) approach to the electronic structure calculations for large approximants. Section IV describes the results for the electronic density of states, including also some closely related crystalline phases in our considerations. We also describe our approach to a ''chemical refinement'' of our structure models. The calculation of the electronic structure is supplemented by total energy calculations allowing to assess the relative stability of the structural variants.

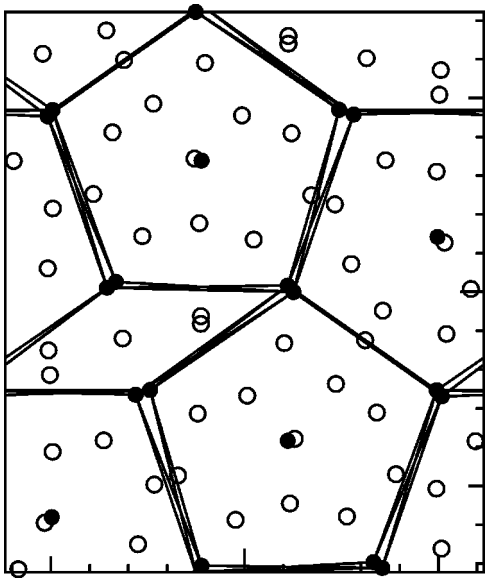

FIG. 1. Projection of the unit cell of orthorhombic $Al_{13}Co_4$ onto the (x,y) plane corresponding to the quasiperiodic plane of *d*-AlNiCo. Empty circles, Al atoms; filled symbols, transition-metal atoms. Note the arrangement of the atoms on pentagonal bipyramidal clusters.

II. ATOMIC STRUCTURE

A. Structural models for decagonal AlNiCo

The starting point of our approach to modeling the structure of *d*-AlNiCo is the structure of the crystalline $Al_{13}Co_4$ compound. The structure of this crystalline phase is supposed to be closely related to the structure of decagonal phase. The structure of $Al_{13}Co_4$ consists of 102 atoms in an orthorhombic unit cell. The coordinates of the atoms in the unit cell have been obtained from the x-ray refinement by Grin.[47] We note that in our previous work on *d*-AlCuCo[43] we used a different model of $Al_{13}Co_4$. The structure of this phase can be viewed as a packing of pentagonal bipyramidal clusters. The unit cell measures 8 Å along the ''periodic'' direction. A projection of the unit cell of $Al_{13}Co_4$ onto the (x,y) plane corresponding to the quasiperiodic plane of *d*-AlNiCo is shown in Fig. 1.

The large number of distinct stable decagonal phases in the *d*-AlNiCo system makes it difficult to model the structure on a systematic basis. The hierarchical organization of the *d*-AlNiCo structure allows to describe the structure in terms of a variety of tilings (or, alternatively, of atomic surfaces in the hyperspace in the cut-and-projection scheme differing

only in the shapes of the outer regions of the hyperatoms). The topological features of each model, i.e., the decoration of the tiles must be chosen in accordance with the information available from diffraction and HREM data.

By a ''model'' we actually mean the list of atomic positions, that are grouped into ''orbits'' with similar atomic environments, up to certain radius; the chemical identity of each orbit which cannot be determined on the basis of the structural data alone is then refined against the features of the calculated electronic DOS and photoemission spectra, under the constraint of fixed overall content of the three species Al, Ni, and Co.

Since the electronic structure is not very sensitive to the medium- and long-range topological order (there is only a small difference between higher-order approximants and the infinite quasicrystal), the different models studied here can be mainly viewed as probing different types of chemical ordering. In the following, we briefly describe three structural models and for each of them different types of chemical order.

Our first model of *d*-AlNiCo is adapted from the model proposed by Henley.[24] This model is characterized by pentagonal bipyramid clusters found already in $Al_{13}Co_4$. The model is based on a rhombus-hexagon tiling and in Ref. 24 the model was called as a neo-Burkov model. In order to avoid confusion with two other Burkov models (B1 and B2) we shall call this model the small-rhombus-hexagon-tiling model (SRHT model). The original Burkov models (B1 or B2) employed in our earlier study of the *d*-AlCuCo (Ref. 43) are problematic because of their too high content of transition metal ($\approx 40\%$). The modification of the Burkov model proposed by Henley allows a larger extent of stoichiometric variations. Instead of the rhombus-hexagon tiling used by Henley, we use the decagonal rectangle-triangle tiling with the same edge length, in which all skinny rhombi are paired into rectangles. This allows us to design a more meaningful parametrization of the structure in terms of the orbits of similar atomic positions, since the radii of both tiles are approximately equal. Our model is constructed as an orthorhombic approximant to the decagonal quasicrystal. It has 340 atoms in the unit cell and its ''quasiperiodic'' dimensions can be viewed as a τ^2-times inflated $Al_{13}Co_4$ cell. A characteristic structural property of this model (as well as of the $Al_{13}Co_4$ structure) is the lack of TM-TM nearest neighbors (TM = transition metal, Ni or Co). For a particular chemical decoration this structure is shown in Fig. 2. As we shall see in Sec. IV it is just this feature of the model that leads to unsatisfactory results for the electronic structure. The photoemission spectra of such an arrangement of atoms show a systematic shift of the position of the main peak to higher binding energies.

In order to investigate the influence of TM-TM neighbors on the resulting photoemission spectra we studied also the crystalline phase $Al_4(NiCo)_3$ with 112 atoms in a cubic cell (space group $Ia\bar{3}d$, Ref. 48). The structure of this phase has no relationship to quasicrystals. The transition metals (TM) Ni and Co are randomly distributed. The content in TM is 42.8 at. %, substantially higher than the 30% in the case of *d*-AlNiCo or 23.5 at. % in monoclinic $Al_{13}(Ni,Co)_4$. Because of large content of TM atoms mutual contacts of TM atoms are inevitable.

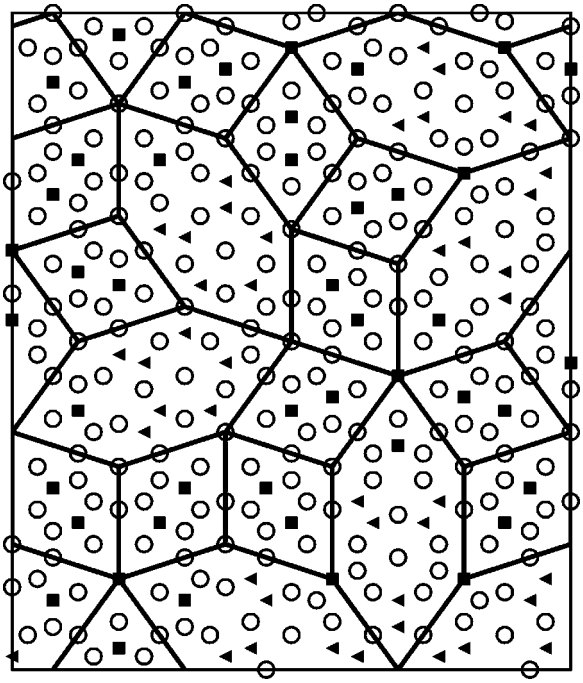

FIG. 2. Projection of the small-rhombus-hexagon-tiling model for the structure of *d*-AlNiCo onto the quasiperiodic plane. The approximant shown here has 340 atoms in the unit cell. The thick lines show the rectangle-triangle tiling (forming rhombi and squeezed hexagons) underlying the construction of the decagonal phase and of its periodic approximants. Empty circles, Al atoms; filled symbols, transition-metal atoms; filled triangles, Ni atoms; filled squares, Co atoms. For the model shown here, only Al and Ni atoms are allowed on the inner rings of the pentagonal bipyramids (cf. text).

Our next model adapted from Hiraga, Sun, and Yamamoto[13] has the following ingredients: clusters with a diameter 20 Å decorate the vertices of a rhombus tiling with an edge length of 20 Å i.e., $\tau\sqrt{\tau+2} \approx 3.08$ times longer than the rhombus edge in the small-rhombus-hexagon-tiling model. We note that the internal structure of the large 20-Å decagonal cluster has been described independently by Steurer and Kuo[5] and Hiraga, Lincoln, and Sun.[6] Placing the decagonal atomic cluster on all vertices of the rhombus tiling leads to a number of short interatomic distances. To avoid these conflicting atomic positions at short distances we put on some vertices only the core part of the large decagonal cluster. The model is presented in Fig. 3. The topology of the model has been optimized using the comparison with diffraction data, see below. We shall call our model the large-rhombus-tiling (LRT) model. Our periodic approximant of this model consists of 1276 atoms in an orthorhombic unit cell; see Table I. It contains 14 decagonal 20-Å clusters.

For a chemical refinement via the electronic structure calculations the model with 1276 atoms is too large. We have therefore considered also a smaller τ-deflated orthorhombic approximant consisting of 484 atoms in the unit cell; see Table I.

B. Large-rhombus-tiling model and the diffraction data

In the case of the large-rhombus-tiling model, the initial guess of the chemical ordering was obtained from the dif-

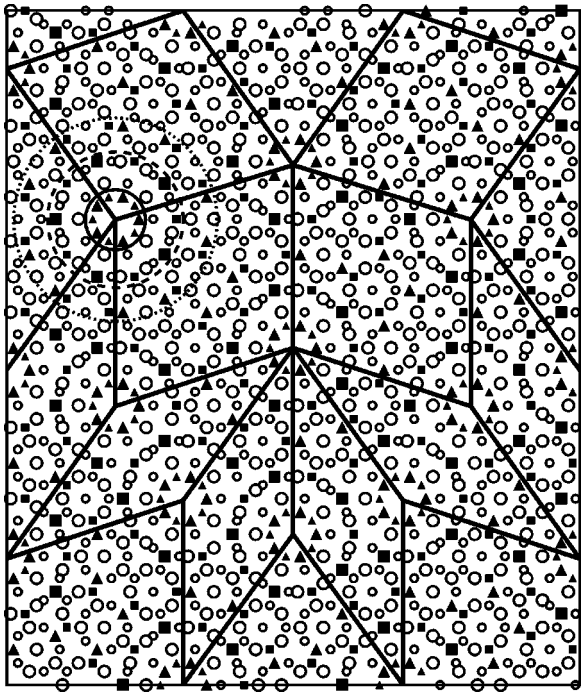

FIG. 3. Projection of the 1276-atom large-rhombus-tiling model for *d*-AlNiCo onto the quasiperiodic plane. The approximant consists of 14 large decagonal clusters. Open circles, Al atoms; filled symbols, transition-metal atoms; filled triangles, Ni atoms; filled squares, Co atoms. The decoration shown here corresponds to the chemical order optimized via electronic structure and total-energy calculations (model V4, cf. text). The black thick line segments show the underlying rhombus tiling. Full, dashed, and dotted circles of larger diameter indicate central, intermediate, and outer part of the decagonal cluster, respectively.

fraction refinement, using 253 independent diffraction intensities measured by Steurer[9] (a more detailed diffraction-refinement study of a similar model is presented in Ref. 49). In contrast to the standard hyperspace refinement approach, the best-fit parameters are determined by the choice of the ''binding'' between atomic decoration and the objects in the tiling. The positional parameters of each decoration orbit bound to a tiling object are allowed to vary only within the constraints imposed by the point-group symmetry of the tiling object. Other parameters associated with the decoration orbit are the chemical occupation and the Debye-Waller (DW) factor.

The nonlinear least-square fit to the diffraction data has been performed using a zero-order model with simplest tiling-decoration binding, in which all atoms were ascribed to a shell of the cluster. In such a model there are 11 distinct

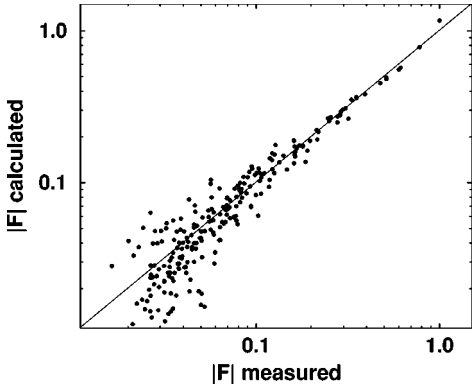

FIG. 4. Log-log plot of the 253 measured and calculated diffraction intensities $|F|$ for the large-rhombus-tiling model of *d*-AlNiCo (experimental data from Steurer, Refs. 9 and 10).

orbits (topological types) of atoms. For each of these we refined two parameters: a mean electron number and the DW factor (for the purpose of this study, the positional parameters were not considered). Since the clusters eventually overlap, in the zero-order model some atoms are accounted for twice. In the diffraction refinement, some orbits were assigned fixed occupation factors (<1) compensating for the fraction of atoms that were placed twice. The model was refined to the weighted *R* factor $R_w = 14.8\%$.

As a next step, from the mean electron numbers obtained from the refinement of the zero-order model, and from the chemical composition constraint, we deduced an optimal chemical ordering, and removed all the conflicting atoms. Then we restarted the diffraction refinement, in which only DW factors and an overall scale factor were refined. The weighted *R* factor of this corrected model slightly decreased to $R_w = 14.1\%$. A log-log plot of the 253 measured[9] and calculated diffraction intensities $|F|$ is presented in Fig. 4.

The electronic structure calculations reported below mainly address the question of the Ni-Co ordering, and include some minor modifications of the Al-TM ordering.

C. Refinement of chemical short-range order

Although from the x-ray diffraction measurements and HREM observations it is possible to deduce some information about the position of aluminum and transition-metal atoms, from the structural data no information about the Ni-Co ordering is available. On the other hand, the photoemission and soft x-ray emission and absorption spectra are sensitive to the local arrangement of transition-metal atoms. This is demonstrated also in Sec. IV of our paper. For each structural model we considered several possible chemical occupa-

TABLE I. Characteristics of our structural models. The table shows chemical composition, number of atoms in the unit cell, and the lattice parameters (in Å).

Model	N_a	*a*	*b*	*c*	note
$Al_4(NiCo)_3$	112	11.396	11.396	11.396	cryst. $Ia\bar{3}d$ (No. 230)
$Al_{13}Co_4$	102	14.452	12.342	8.158	Grin *et al.* (Ref. 47)
$Al_{0.738}(NiCo)_{0.262}$	340	37.779	32.136	4.080	$\tau^2 \times Al_{13}Co_4$, SRHT
$Al_{0.705}(NiCo)_{0.295}$	484	44.232	37.626	4.080	LRT
$Al_{0.709}(NiCo)_{0.291}$	1276	71.569	60.880	4.080	LRT

tions of different topological sites. From the comparison of the calculated DOS with experimental photoemission curves we could exclude some variants of the structural models. After some attempts we have succeeded to find a model which provides a reasonable agreement of the electronic structure with experiment. We checked the correctness of this refinement also by the calculation of the total energy of each chemical variant of the model. We have found out that the optimal model obtained by the chemical refinement exhibits also the lowest total energy.

III. SELF-CONSISTENT TIGHT-BINDING LMTO METHOD

As quasicrystals are typically multicomponent systems, a self-consistent calculation of the electronic structure is necessary. This is particularly significant in the case of quasicrystals containing two different transition metals since the interaction of the transition-metal atoms leads to significant changes of the position and width of the *d* bands of the two transition metals[44–46] during the self-consistent iterations. We shall see in Sec. IV that this effect is really important for obtaining satisfactory agreement of the calculated positions of the *d* bands with experiment. As quasicrystals are ordered systems, the number of locally topologically nonequivalent sites is limited (within a finite cutoff radius, see Sec. II A)—in our models we consider up to 38 topologically different sites.

The most efficient procedure to obtain self-consistency in a system with a limited number of topologically inequivalent sites is the real-space recursion method.[50] The recursion method is very efficient to obtain self-consistency and to get the gross features of the electronic structure. The accuracy of the recursion method is sufficient during self-consistent iterations as integral quantities only are relevant for the construction of the new charge density. The accuracy of the method is also satisfactory for the purpose of comparison of the calculated electronic structure with the experimental data.

For the calculation of the electronic structure we used the tight-binding linear muffin-tin orbital (TB-LMTO) method.[51,52] The TB-LMTO Hamiltonian is transformed from the standard LMTO basis to the most localized tight-binding basis. Some details of the application of the TB-LMTO formalism to quasicrystalline approximants are given also in our previous papers.[53] The LMTO structure constants are calculated for each atomic site, including all neighbors within a sphere containing 20 atoms on average. For the construction of the starting Hamiltonian we used as the initial potential parameters values tabulated for the pure metals. The two-center TB Hamiltonian in the Löwdin orthonormal representation is determined in terms of an expansion in powers of the nonorthogonal TB Hamiltonian in the screened, most localized basis and of the overlap matrix. This expansion is truncated at the second-order term. The local densities of states (DOS) of all topologically nonequivalent atoms are calculated using the recursion method.[50] The local DOS was obtained by summation over contributions from *s*, *p*, and *d* orbitals. We used typically 20 recursion levels and the Lucchini-Nex terminator.[54] The valence-charge density of an atom is reconstructed from the moments of the local DOS. The core-charge density is obtained from relativistic self-consistent calculation of free atoms. The Madelung constants are calculated by the Ewald summation technique. The Kohn-Sham potential is constructed within the local-density approximation (LDA). For the exchange-correlation potential the Barth-Hedin formula is used.[55] For all topologically nonequivalent sites we iterated charge densities to self-consistency.

We performed the calculation in real space, i.e., only for the Γ point in the Brillouin zone. As the Brillouin zone of a decagonal quasicrystal with 4-Å periodicity is quite extended along the periodic axis, the dispersion along this direction cannot be neglected. We constructed a supercell containing three elementary cells stacked along the periodic direction containing together 1452 atoms. Such a multiplication of the elementary cell does not increase the number of topologically nonequivalent sites and the computer time scales linearly with the total number of atoms in the supercell. The energy resolution depends on the number of recursion levels, which is, however, limited by the size of the model. At the end of the self-consistent iterations we increased the energy resolution by increasing the number of the recursion levels to 50. We increased correspondingly the size of the model by multiplication of the elementary unit cell to $9\times484=4356$ atoms. Such increased accuracy has been used also for the total-energy calculations.

As all our approximants are finite and periodic in real space even in quasiperiodic directions we do not have problem with **k** as quantum numbers. However, size of the Brillouin zone of our approximants in quasiperiodic directions is very small: 0.02–0.03 $Å^{-1}$. In quasiperiodic limit the size of Brillouin zone would shrink to zero. Therefore the approximation of Γ point (i.e., $\mathbf{k}=0$) in the quasiperiodic directions is quite satisfactory.

The total density of states (DOS) was calculated by summation over the local DOS. We calculated the total DOS also by the recursion technique utilizing randomly phased vectors as the initial vectors. Good convergence between both approaches was achieved. This proves that the choice of a restricted number of nonequivalent sites in the models with large unit cells is sufficiently representative.

The aim of our work is to find a model of atomic structure of decagonal AlNiCo quasicrystal, particularly its short-range order, that is consistent with available diffraction, photoemission, and soft x-ray spectroscopic data. We assume that for this purpose the accuracy of our electronic structure calculations is quite sufficient. In this paper we do not address the problem of character of the electronic states of a true quasiperiodic system. We refer readers interested in this problem to Ref. 56. As gross features of the electronic structure are determined by the short-range order we assume that sizes of approximants used as models of decagonal AlNiCo are sufficiently representative.

IV. ELECTRONIC STRUCTURE OF DECAGONAL Al-Ni-Co

A. Relation to crystalline phases

The electronic structure of orthorhombic $Al_{13}Co_4$ was obtained by **k**-space TB-LMTO calculations, using 240 **k** points in a quarter of Brillouin zone. Figure 5 shows the total and partial Al and Co densities of states. The most striking feature in the electronic structure is the deep DOS minimum

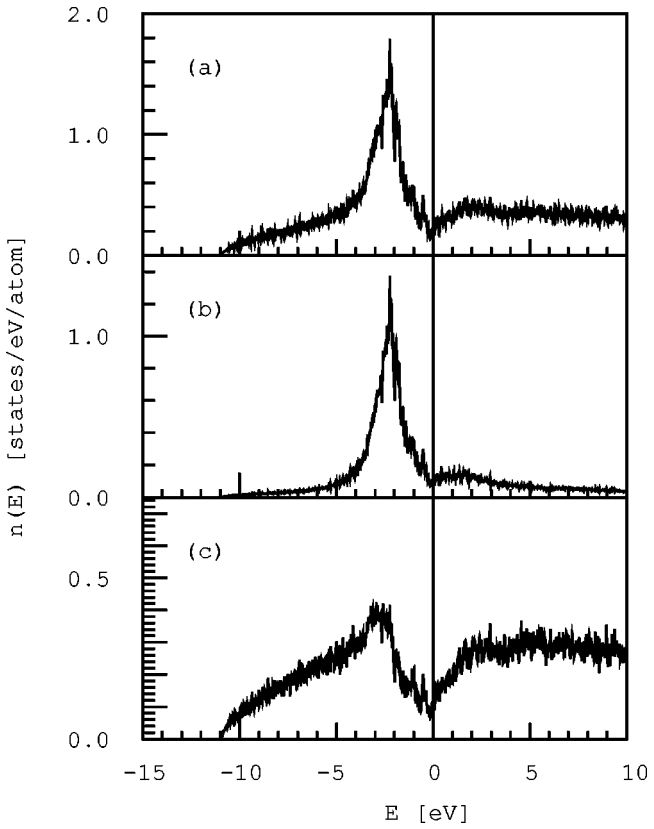

FIG. 5. Total and partial densities of states of orthorhombic $Al_{13}Co_4$, calculated for the crystal structure determined by Grin (Ref. 47). Total DOS (a), Co (b), and Al (c).

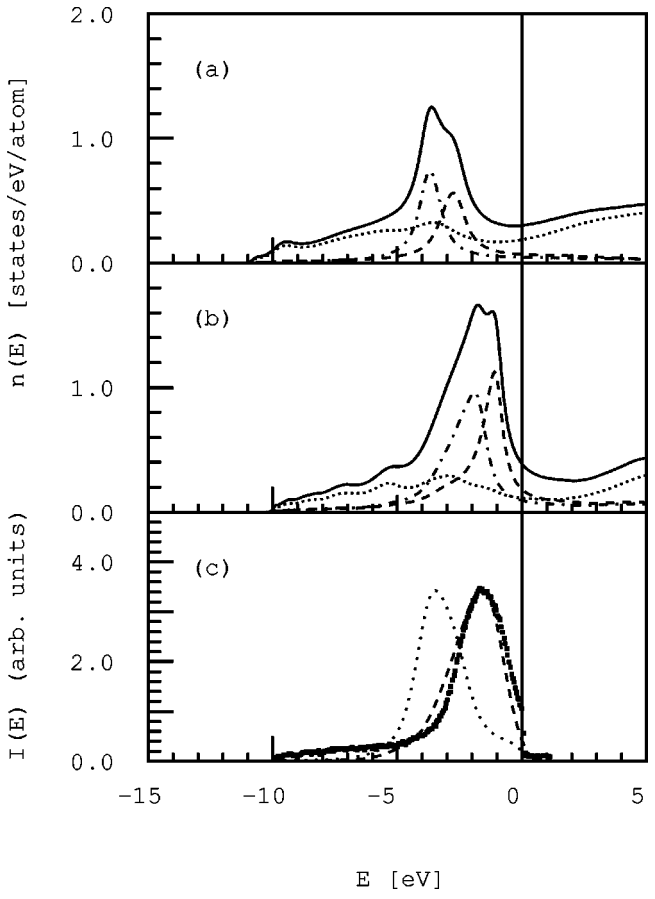

FIG. 6. Total and partial densities of states of orthorhombic $Al_{13}(Ni_{0.5}Co_{0.5})_4$ (a) and of cubic $Al_4(Ni_{0.5}Co_{0.5})_3$ (b) with a random distribution of Ni and Co atoms. The calculated photoemission spectrum of $Al_{13}(Ni_{0.5}Co_{0.5})_4$ (dotted curve) and $Al_4(Ni_{0.5}Co_{0.5})_3$ (dashed curve) is compared in (c) with photoemission data of decagonal $Al_{70}Ni_{15}Co_{15}$.

very close to the Fermi level, resulting from a broad structure-induced minimum in the partial Al DOS (whose lower part is, however, largely covered by the Co-*d* band) and a weak hybridization gap at the upper edge of the Co-*d* band.

The main contribution to the photoemission intensity comes from the *d* electrons of the transition metals. A comparison of the position of Co-*d* peak (≈ -2.4 eV) with the position the main peak in photoemission data (≈ -1.8 eV) (Refs. 37–39) of *d*-AlNiCo shows a significant shift of the *d* band of the decagonal phase towards the Fermi level, indicating a substantial difference in the electronic structures of crystalline $Al_{13}Co_4$ and the decagonal phase.

The first attempt to simulate the electronic structure of the *d*-AlNiCo was done by replacing Co by a random mixture of Co and Ni atoms. The resulting DOS and the corresponding photoemission spectrum (PES) calculated by the recursion method is presented in Figs. 6(a) and 6(c). The position of the Co-*d* band is shifted to somewhat higher binding energy (-2.8 eV), but the mutual position of Co- and Ni-*d* bands exhibits clear splitting which is not seen in the experimental photoemission data.[37–39] The calculated PES has unimodal shape peaked at ≈ -3.7 eV. The position of the peak is in significant disagreement with the experiment; see Fig. 6(c).

The position of the Co- and Ni-*d* peaks in the *d*-AlNiCo phase as seen in the experimental photoemission and soft x-ray data is really remarkable. Soft x-ray spectroscopy[40] shows that both peaks are located at low-binding energies, apparently very close to each other. From the photoemission data is not possible to distinguish separate peaks. There is no splitting of the *d* bands as in the case of *d*-AlCuCo.[43] The splitting of the Cu- and Co-*d* bands and particularly the shift of the fully occupied Cu-*d* band to lower energies was interpreted as a stabilizing mechanism for the quasicrystalline phase. Such a mechanism does not work in the case of *d*-AlNiCo phase as it is clearly seen from the experimental data.[37–40]

Figures 6(b) and 6(c) show the total, partial DOS's and PES of crystalline $Al_4(TM)_3$ (the crystallographic data are given in Ref. 48). The transition metals (TM) Ni and Co are randomly distributed. The content in TM is 42.8 at. %, substantially higher than the 30% in the case of *d*-AlNiCo or the 23.5 at. % in $Al_{13}(Ni,Co)_4$. Because of the large content of TM atoms, mutual contacts of TM atoms are inevitable. Although the structure of this phase has no relationship to quasicrystals the position of the Ni and Co *d* bands agrees much better with the spectroscopic results for the quasicrystal than for the random $Al_{13}(Ni,Co)_4$ phase. The main difference is that in $Al_{13}(Ni,Co)_4$ no TM-TM nearest neighbors are allowed. We take this as an indication that the correct chemical decoration of *d*-AlNiCo must contain a substantial number of TM-TM nearest-neighbor pairs.

B. Small-rhombus-hexagon-tiling model

The electronic structure of the SRHT model of *d*-AlNiCo, which has a τ^2-times inflated unit cell of $Al_{13}Co_4$ in the

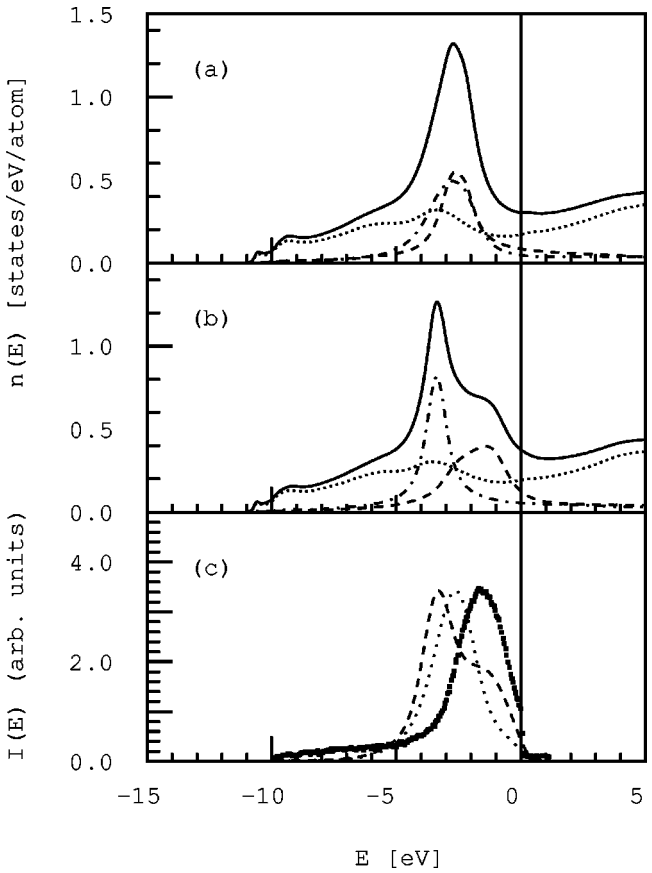

FIG. 7. (a) Total and partial densities of states of *d*-AlNiCo for the 340-atom small-rhombus-hexagon-tiling model with chemical decoration shown in Fig. 2. (b) As in (a), but the occupation with Ni and Co atoms has been interchanged. (c) Photoemission intensities calculated from (a) and (b) compared with the experimental data of Stadnik and co-workers (Ref. 39).

quasiperiodic plane, but only 4.08-Å periodicity along the periodic axis was calculated for many different chemical decorations in an attempt to achieve agreement in the position of the *d* peaks of TM atoms with experiment. We failed to get a satisfactory agreement for any of the tested configurations. The electronic structure of all models exhibits a systematic shift by at least 0.5 eV to lower energies. Moreover, many configurations provide split *d* bands. Figure 7 shows the calculated total and local DOS's and the photoemission intensity for the decoration presented in Fig. 2 and for an alternative model with interchanged Co and Ni occupancy, compared with the experimental data.[37–39] While for the first configuration the DOS shows unimodal character, for the latter configuration we find a pronounced splitting of the TM *d* bands. Ni and Co atoms are similar in size and therefore exchangeable; in x-ray experiments they are indistinguishable and also in most of the structural models the difference is ignored. However, Fig. 7 shows that in *d*-AlNiCo atoms Ni and Co exhibit a substantially different chemical behavior and cannot be arbitrarily exchanged.

C. Large-rhombus-tiling model

This model differs from the previous ones by the presence of large 20-Å clusters (cf. Figs. 2 and 3). We shall see below

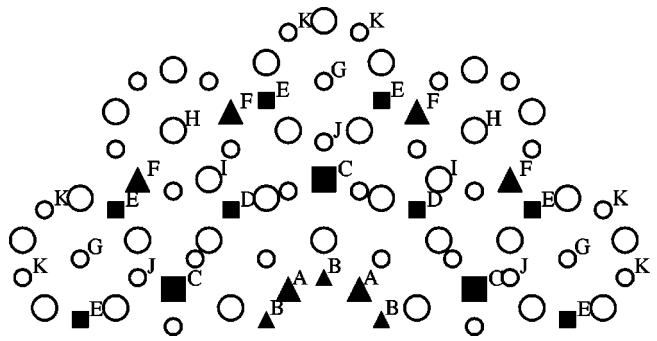

FIG. 8. Projection of part of the 20-Å decagonal cluster onto quasiperiodic plane. The chemical decoration shown here corresponds to the version V4. Open circles, Al atoms; filled symbols, transition-metal atoms; filled triangles, Ni atoms; filled squares, Co atoms. Occupation of the sites marked by labels A–K was optimized via the electronic structure calculations.

that these clusters are essential for obtaining a satisfactory agreement of the calculated photoemission intensities with experimental data. The electronic structure is determined largely by the local arrangement of atoms. For the purpose of the self-consistent TB-LMTO calculations we distinguish 38 crystallographically inequivalent positions. For each of these sites the LMTO structure constants are calculated and the potential parameters are iterated to self-consistency.

From the comparison of the electronic structure of the two crystalline phases $Al_{13}Co_4$ and $Al_4(TM)_3$ and their local arrangement of atoms it is possible to deduce that the SRHT model provides an incorrect position of the *d* peaks because of the lack of close contacts among TM atoms. However, such contacts can exist if we occupy the central part of the large decagonal cluster by fivefold rings of TM atoms. The rings of TM atoms must exist in both planes—flat and puckered—along the periodic direction forming thus a columnar cluster of TM atoms. As the flat and puckered layers of atoms are related by a tenfold screw axis, in the projection onto the quasiperiodic plane the two fivefold rings form a tenfold ring of TM atoms. Such a ring of TM atoms is seen also in the Burkov model[21] as well as in the recent model of Yamamoto and Weber.[22] The presence of TM atoms in both layers along the periodic direction turns out to be essential. If the central cluster is occupied by alternating Al and TM rings as it was proposed in the older work of Yamamoto, Weber, and Tsai[25] or as it is seen in the recent proposal of Steurer, Honal, and Haibach,[15] the resulting electronic structure is in the same disagreement with the photoemission data as it was observed for the previous SRHT model; see Fig. 10 and below. On the other hand, if one attempts to occupy the fivefold rings in the SRHT model by TM atoms only, the stoichiometry of the system would be substantially changed. The constraint of maintaining the correct stoichiometry makes the optimization of the chemical order a quite complex task. We have tested altogether 17 different chemical configurations. In order to simplify the presentation of the results we shall divide the process of optimization into two parts: first the optimization of the chemical occupation of the sites in the central part of the 20-Å clusters is discussed, second we present the results of optimization of decoration of the outer shells; see Fig. 3.

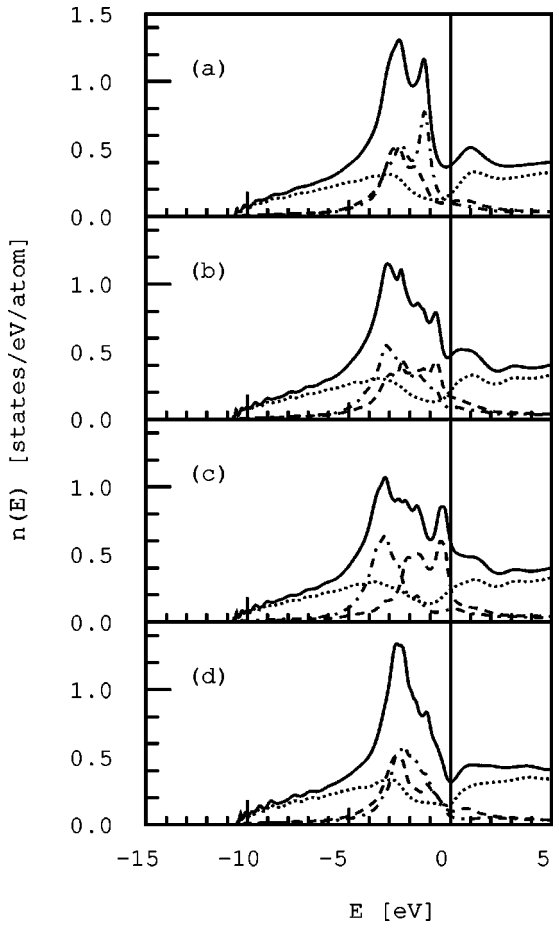

FIG. 9. Total and partial densities of states of *d*-AlNiCo calculated for the 484-atom model and four different chemical decorations differing mainly in the occupation of the innermost ring of the 20-Å cluster (see Table II), Ni ring, model V4 (a); Ni-Co ring, model V5 (b); Co ring, model V6 (c); and Al-Ni ring, model V7 (d). Total DOS, full line; Al-DOS, dotted line; Ni DOS, chain line; Co-DOS, dashed line.

1. Optimization of chemical order in the central part of 20-Å cluster

We have considered a large number of different possibilities for the occupation of the central ring in the large 20-Å cluster by TM atoms; only four of them are discussed here: Ni ring (model V4), Ni-Co ring (V5), Co ring (V6), and Al-Ni ring (V7). Although in the electronic structure calculation we actually distinguish 38 topologically different sites in the unit cell we restrict the discussion only to the sites in a single 20-Å decagonal cluster. Figure 8 shows one-half of the decagonal cluster with the chemical decoration corresponding to version V4. We varied the chemical occupation of the sites marked in Fig. 8 by labels A–K. A description of models V4 to V7 is given in Table II. In versions V4 and V6 the inner ring (positions A and B) is occupied by Ni or Co atoms only. In order to achieve the correct composition, the second shell (positions C and D) must then be occupied by TM atoms of the other species as the inner ring. V5 contains a mixed Ni-Co columnar cluster (Ni and Co atoms in alternating planes). This leads also to a mixed occupation with Ni and Co on the second (C and D) and third (E and F) shells. Version V7 allows for a mixed Al-TM (here Al-Ni) occupation of the inner ring, to maintain the correct stoichiometry, part of Ni atoms must then be placed on some of the outer sites (here sites H in the centers of the small rings arranged around the large central ring). The partial coordination numbers for all models are summarized in the lower part of Table II. Note in particular the large variations in the TM-TM and Al-TM coordination numbers.

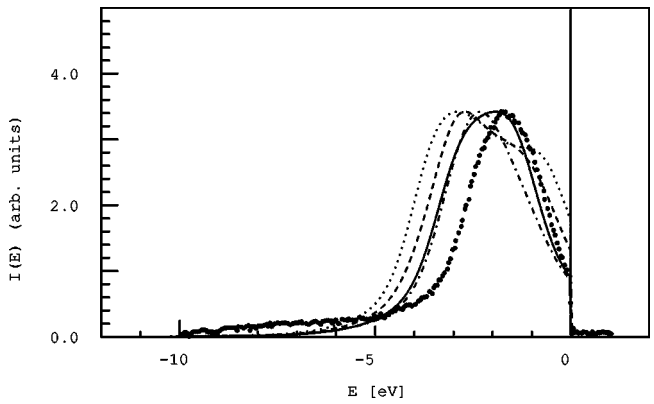

FIG. 10. Photoemission intensities of *d*-AlNiCo calculated for the 484-atom model and four different chemical decorations differing in the occupation of the outer part of the 20-Å cluster (see Table II), Ni ring, model V4 (full line); Ni-Co ring, model V5 (dashed line); Co ring, model V6 (chain line); Al-Ni ring, model V7 (dotted line), compared with experiment (Ref. 39).

Figure 9 shows the total and partial densities of states, Fig. 10 the calculated photoemission spectra (PES) compared with the experimental data. The most distinct differences between these models appear at the level of the positions and shapes of the Co- and Ni-*d* bands. In all models except V4 with the Ni ring in the central part of the cluster, the Ni-3*d* band lies at higher binding energies than the Co-3*d* band—as expected from the band filling in the pure metals. Only the model V4 behaves differently: the Co-3*d* band is pushed down to higher binding energies than the Ni-3*d* band. A possible explanation is a high degree of Co-Al hybridization—in agreement with the high Co-Al coordination number. It is interesting to confront this result with experiment. The most accurate information on the structure of the valence band comes from PES (which, however, cannot differentiate between Ni and Co bands). For the calculation of the PES, the photoionization cross sections tabulated by Yeh and Lindau[57] and a modest Gaussian broadening of 0.3 eV to simulate experimental resolution have been used. To demonstrate the importance of TM rings as discussed in the previous section, the case of the Al-Ni ring (model V7) is here also presented. For the model with a mixed Ni-Al ring leading to a high TM-Al coordination on both Ni and Co sites we find a unimodal, symmetric *d*-band DOS peaked at about -2.3 eV. For the model with an inner Co ring (V6) leading to a high Ni-Al, but low Co-Al coordination, high Co-Co coordination, no Ni-Ni neighbors at all we find a bimodal asymmetric *d*-band DOS with a peak at about -3.0 eV, compared to a symmetric unimodal PES intensity peaked at -1.8 eV.

The best—but far from perfect—agreement with experimental data is obtained for the Ni ring (model V4) which has just opposite characteristic (cf. Table II). The PES intensity distribution corresponding to the mixed Ni-Co ring (model

TABLE II. Properties of the large-rhombus-tiling model for various variants of occupation of the central ring in the decagonal cluster. Position of the topological sites A–K seen in Fig. 11. In the table there are listed occupation of the topological sites, chemical composition, coordination numbers, and the calculated total energies.

Top. site/model	V4 (Ni ring)	V5 (Ni-Co ring)	V6 (Co ring)	V7 (Al-Ni ring)
A	Ni	Ni	Co	Ni
B	Ni	Co	Co	Al
C	Co	Ni	Ni	Co
D	Co	Co	Ni	Co
E	Co	Co	Ni	Co
F	Ni	Ni	Co	Ni
G	Al	Al	Al	Ni
H	Al	Al	Al	Ni
I	Al	Al	Al	Al
J	Al	Al	Al	Al
K	Al	Al	Al	Al
Content of Al (%)	68.60	68.60	68.60	71.07
Content of Ni (%)	16.52	15.70	14.88	14.05
Content of Co (%)	14.88	15.70	16.52	14.88
Coord. no. Al-Al	11.87	11.87	11.87	11.27
Coord. no. Al-Co	2.44	2.04	1.62	2.30
Coord. no. Al-Ni	1.62	2.03	2.44	2.08
Coord. no. Co-Al	10.72	9.02	7.25	10.44
Coord. no. Ni-Al	7.25	8.76	10.72	10.79
Coord. no. Co-Co	0.00	0.79	4.50	0.00
Coord. no. Co-Ni	0.55	2.10	0.50	0.83
Coord. no. Ni-Co	0.50	2.10	0.55	0.88
Coord. no. Ni-Ni	4.50	0.79	0.00	1.41
Heat of formation (eV/atom)	−0.36	−0.31	−0.23	

V5) shows a clear splitting of the *d* bands with one shoulder shifted to lower binding energy. Analysis of these results demonstrates that it is mainly a high Ni-Al coordination number which leads to a shift of the *d* band to higher energies. The best agreement with the experimental spectrum is obtained for a decoration resulting in a high Ni-Ni and Co-Al coordination.

2. Optimization of chemical order in the outer part of 20-Å cluster

Most of the HREM studies and image contrast simulations for *d*-AlNiCo confirm the occupation of the core part of the 20-Å decagonal cluster by transition-metal atoms.[29] However, there is much less consensus concerning of the outer part of the cluster. Structural models for the decagonal cluster proposed by Steurer and Kuo,[5] Hiraga, Lincoln, and Sun[6] and Burkov[20] are identical with respect to the central part of the cluster, but disagree in their outer part. From stoichiometry considerations it follows that this outer part should contain ≈20 transition-metal atoms. The possible arrangement of these atoms was the next subject of our study. The simplest possibility is to place them regularly on the small rings such as to form a decagonal ring of large diameter. Some of the considered chemical versions of the models denoted as V42–V46 are listed in Table III. Figures 11 and 12 show a comparison of the calculated DOS's and photoemission spectra with experimental data. The results again show a high sensitivity of the resulting PES to small changes in chemical short-range order (versions V42 and V44 differ only by interchanging the occupation of sites E and F with Ni and Co, respectively). Versions V42–V45 correspond to various variants of the outer decagonal ring of 20 TM atoms. It is interesting that the best agreement with experiment was obtained for the version V46 in which the decagonal symmetry of the the outer ring of TM atoms is broken. We note that compared to version V4 (=V42) the chemical refinement of the outer part of the large cluster leads to a further increase of the Co-Al and Ni-Ni coordinations. The broken symmetry of the outer ring might be taken as an indication that the chemical arrangement in this region of the structure is possibly disordered. However, this conjecture could be tested only by calculation on larger models with a vastly increased number of inequivalent sites.

3. Total-energy calculation

It is generally accepted that the electronic structure plays an important role in stabilization of quasicrystalline structure. In the case of icosahedral quasicrystals the dominant contribution to the stability comes from the structure-induced pseudogap in the density of states at the Fermi level. The pseudogap lowers the band energy of the system. In the case

TABLE III. Properties of the large-rhombus-tiling model for various variants of occupation of the outer part of the decagonal cluster. Position of the topological sites A–K seen in Fig. 11. In the table there are listed occupation of the topological sites, chemical composition, coordination numbers, and the calculated total energies.

Top. site	V42	V43	V44	V45	V46
A	Ni	Ni	Ni	Ni	Ni
B	Ni	Ni	Ni	Ni	Ni
C	Co	Co	Co	Co	Co
D	Co	Co	Co	Co	Co
E	Co	Co	Ni	Al	Al
F	Ni	Al	Co	Co	Al
G	Al	Al	Al	Ni	Al
H	Al	Ni	Al	Al	Al
I	Al	Al	Al	Al	Ni
J	Al	Al	Al	Al	Al
K	Al	Al	Al	Al	Co
Content of Al (%)	68.60	71.07	68.60	70.66	70.66
Content of Ni (%)	16.52	14.05	16.52	14.46	14.46
Content of Co (%)	14.88	14.88	14.88	14.88	14.88
Coord. no. Al-Al	11.87	11.93	11.87	11.92	11.90
Coord. no. Al-Co	2.44	2.47	2.38	2.43	2.16
Coord. no. Al-Ni	1.62	1.38	1.68	1.44	1.43
Coord. no. Co-Al	10.72	11.27	10.72	11.27	11.11
Coord. no. Ni-Al	7.25	7.05	7.25	7.28	7.28
Coord. no. Co-Co	0.00	0.00	0.00	0.00	1.00
Coord. no. Co-Ni	0.55	0.00	0.55	0.00	0.27
Coord. no. Ni-Co	0.50	0.00	0.50	0.00	0.28
Coord. no. Ni-Ni	4.50	5.29	4.50	5.14	5.14

of decagonal quasicrystals the situation is more complicated. In the case of d-AlCuCo the pseudogap which exists in the Al-(s,p) bands is covered by the Co-d band overlapping with the Fermi level and the main stabilizing contribution comes from the mutual interaction of the transition-metal atoms which leads to split of Cu- and Co-d bands and consequently a shift of the fully occupied Cu-d band to high binding energies.[43] Using the same mechanism in the case of d-AlNiCo one should conclude that the variant of the model with Al-Ni ring is the most stable out of all considered variants. However, the comparison with the experimental spectroscopic data does not support such a conclusion. In order to understand this contradiction we have attempted to calculate the total energies of the systems. However, one must realize that as our d-AlNiCo models differ in composition, a calculation of their total energies is not sufficient to decide the question of relative stability—to do this one would have to take the neighboring crystalline phases into account and perform the usual double-tangent construction to get this part of the phase diagram. Therefore we have considered only the models V4, V5, and V6 which have the same Al content and differ only in the occupation of the central ring and in the Co/Ni ratio. Even then a total-energy calculation for such a large system is a formidable task. Exact diagonalization in **k** space continued iteratively to full self-consistency is excluded in practice. Real-space recursion calculation is much faster converged with respect to self-consistency, but very difficult to converge with respect to the size of the supercell. This is largely a consequence of the shape of the unit cell of the decagonal approximants, with a small cell parameter in one and large dimensions in the other directions (aspect ratio 1:9). In the present case we have extended the calculations to supercell consisting of nine conventional cells stacked in the periodic direction (i.e., 4356 atoms/supercell). With this setting we estimate the total energies to be converged to within ± 0.025 eV/atom. The total energy in addition to the band energy includes also the contributions from the double-counting terms, the exchange energy, and the Madelung energy. The results are included in Table II (we give here the heat of formation). Surprisingly, the model with Ni ring in the center of the large cluster has the lowest total energy and not the variants with the Co ring or Ni-Co ring which have apparently a lower band energy. This result is in agreement with our previous conclusion that the best agreement with the photoemission data is provided by the model with the Ni ring in the center of the large cluster.

4. Comparison with soft x-ray data

Contrary to the photoemission data which cannot distinguish separate Ni and Co contributions in the soft x-ray spectra (SXS) one can see contributions from each chemical type and each orbital symmetry separately. Figure 13 compares the calculated s-d contributions for our model with the Ni ring with the experimental data.[41] The SXS spectra confirm the surprising reversal in the positions of the Co-3d and Ni-3d bands (note that this was not the case in the earlier publication[40]). We also note that the d-band peaks in the SXS spectra occur at somewhat higher binding energies in

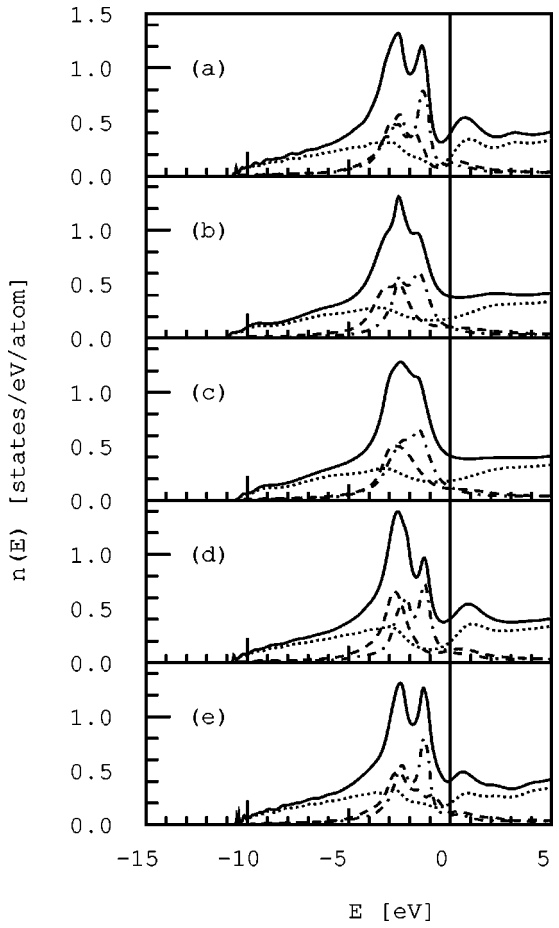

FIG. 11. Total and partial densities of states of *d*-AlNiCo calculated for the 484-atom model and four different chemical decorations differing mainly in the occupation of the outer part ring of the 20-Å cluster (see Table III), model V42 (a), model V43 (b), model V44 (c), models V45 and V46 (d). Total DOS, full line; Al DOS, dotted line; Ni DOS, chain line; Co DOS, dashed line.

the PES spectra—and are thus in better agreement with our results.

5. Large approximant

After optimizing the topological structure via diffraction refinement, see Sec. II B, and finding the optimal chemical short-range order by electronic structure calculations for the medium-sized models, we have calculated also the electronic structure of our largest approximant. It contains 1276 atoms in the unit cell and its 14 large decagonal clusters are linked with both types of linking. Figure 14 shows a comparison of the calculated total and partial DOS's and photoemission spectra of the large and smaller models. As the gross features of the electronic structure is determined predominantly by the local arrangement of atoms a big difference in the electronic structure of both models could not be expected.

The local densities of states have been analyzed on the 38 sites that have been considered as topologically inequivalent in our model V42. We recognize some interesting features: while a certain depression of the local DOS's is recognizable on all Al sites, the depth of this pseudogap varies considerably from site to site. The Ni DOS is split. The main peak is close to -1.4 eV, the minor subpeak is at -2.5 eV. The

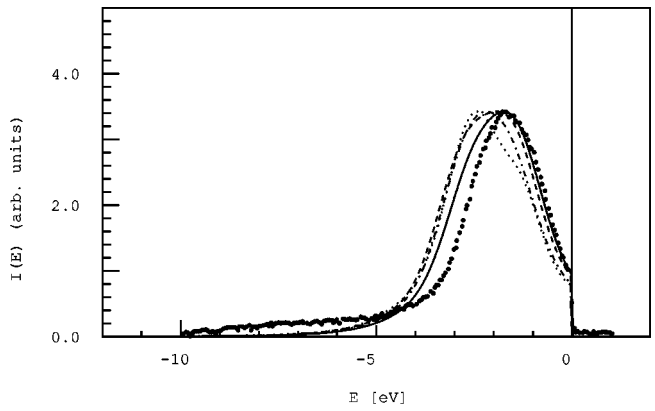

FIG. 12. Photoemission intensities of *d*-AlNiCo calculated for the 484-atom model and five different chemical decorations differing only in the occupation of the outer part of the 20-Å cluster (see Table III), model V42 (dashed line), model V43 (chain line), model V44 (dotted line), model V45 (double dot line), and model V46 (full line) compared with experiment.

Ni-*d* band shows only a small overlap with the Fermi level. The Co DOS is peaked around -2.5 eV, it consists of relatively sharp main peak and a shoulder close to the Fermi energy. The larger width of the Ni-*d* band reflects the higher Ni-Ni coordination, the structure of Co band is the consequence of the high Co-Al coordination and therefore strong Co-*d*–Al-(s,p) hybridization.

V. CONCLUSIONS

We have presented a very detailed theoretical study of the atomic and electronic structures of *d*-AlNiCo. Not surprisingly, this turned out to be an exceedingly complex task. While it is possible to discriminate among the various structural models that have been proposed in the literature on the basis of the available diffraction and HREM data, and even to proceed to a topological optimization of the most promising models based on the presence of large 20-Å decagonal clusters, the existing experimental information does not allow us to specify the chemical decoration. In our study we have undertaken an attempt to optimize the chemical order on the basis of electronic structure calculations and comparison with data from photoemission and soft x-ray spectroscopy, following the strategy that turned out to be successful for *d*-AlCuCo.[43] The comparison of the calculated electronic structure with experiment confirms our choice of the LRT model, but the chemical order is shown to induce large variations in the spectra. In a first step we have been able to show that the decoration of the innermost part of the 20-Å cluster with pentagonal Ni rings leads to the relatively best agreement. The decisive factors are large Ni-Ni and Co-Al coordination numbers inducing a relatively broad Ni-*d* band and strong Co-*d*–Al-(s,p) hybridization. The agreement can be further improved by an appropriate decoration of the outer parts of the ring, inducing a certain local disorder. This is again reflected in a further increase of the Ni-Ni and Co-Al coordinations. A surprising outcome is that the peak in the Co-*d* band is pushed down to higher binding energies than the peak in the Ni-*d* band. This is contrary to the positions expected from the relative *d*-band filling and occurs only for

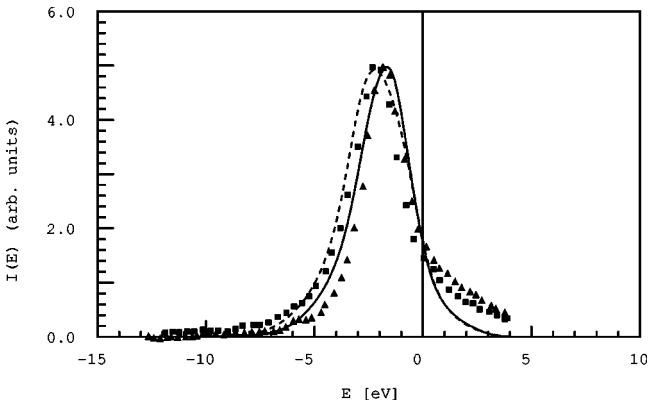

FIG. 13. Calculated soft x-ray spectra for Ni-3d band (full line) and Co-3d band (dashed line) compared with experimental data: triangles, Ni-3d band; squares, Co-3d band.

the optimized decoration of the decagonal phase and not in any other of the decorations or in other crystalline AlNiCo phases studied in this work. Total-energy calculations confirm that the optimized decoration also leads to the lowest total energy (at fixed Al/TM composition), the reversal of the band positions is also confirmed by soft x-ray spectroscopy.

It is certainly also surprising that the atomic and electronic structures of the d-AlNiCo are so different from those of d-AlCuCo. The essential point is the different strength of the Cu-Cu and Ni-Ni interactions: In d-AlCuCo the Cu-Cu interaction is largely repulsive and this leads to a structure with no Cu-Cu contacts (in 5D picture of the structural model Cu atoms are located in the center of the acceptance domain) and a strong repulsion between the Cu- and Co-d bands, pushing the Co band towards the Fermi level and the Cu band down to higher binding energies. The TM-d–Al-(s,p) hybridization is weak for both metals. In d-AlNiCo the Ni-Ni and Co-Al interaction is attractive, leading to strong Ni-Ni and Co-Al coordination and to lowering of the energy of the Ni band. A further important difference is that the number of Ni-Co pairs is much lower than the Cu-Co coordination numbers—this largely eliminates the d-band repulsion which is so characteristic for d-AlCuCo.

However, it must be pointed out that the results presented here all refer to almost the same composition around $Al_{70}Ni_{15}Co_{15}$. Variations in the Ni/Co ratio could affect the picture we have sketched here quite appreciably—a high Ni-Ni coordination cannot be a decisive factor. This is certainly one of the factors behind the bewildering structural

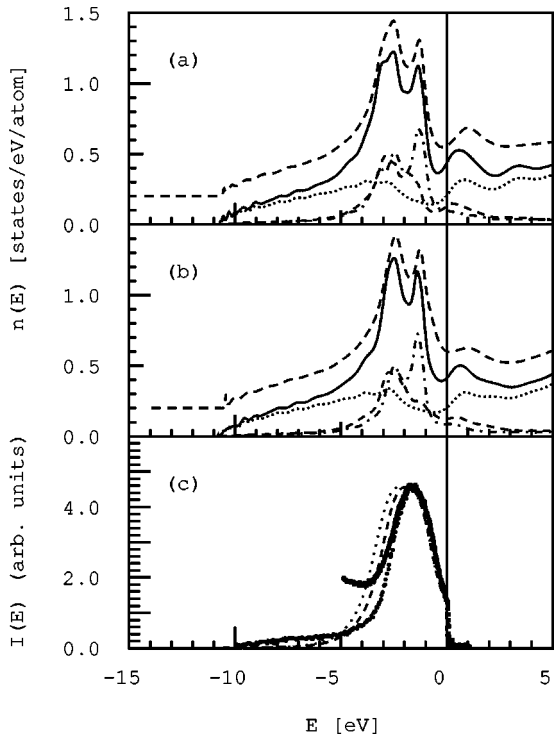

FIG. 14. The total and partial densities of states of two variants V42 (a) and V46 (b) of the 1276-atom model. Total DOS, full line; Al DOS, dotted line; Ni DOS, chain line; Co DOS, dashed line. The shifted dashed lines represent the total DOS of the corresponding 484-atom models. Panel (c) compares the calculated photoemission intensities for the V42 (dotted line) and V46 (dashed line) models with two sets of experimental data, squares, Ref. 38; full circles, Ref. 39.

complexity of d-AlNiCo. However, further studies will be necessary to bring a final assessment.

Further studies based on this model will concentrate on the electronic transport properties of d-AlNiCo, with the aim of finding out how the difference in the electronic structure affects the anisotropy of the transport properties.

ACKNOWLEDGMENTS

We thank Professor Esther Bellin-Ferré for enlightening discussions and for communicating unpublished material. This work has been supported by the Austrian Ministery for Science and Transport within the Materials Research Program. M.K. also thanks for support the Grant Agency for Science of Slovakia (Grant No. 2/6064/99).

[1] D. Shechtmann, I. Blech, D. Gratias, and J. W. Cahn, Phys. Rev. Lett. **53**, 1951 (1984).
[2] L. A. Bendersky, Phys. Rev. Lett. **55**, 1461 (1985).
[3] L. X. He, Y. L. Wu, and K. H. Kuo, J. Mater. Sci. Lett. **7**, 1284 (1988).
[4] A. P. Tsai, A. Inoue, and T. Masumoto, Mater. Trans., JIM **30**, 300 (1989).
[5] W. Steurer and K. H. Kuo, Acta Crystallogr., Sect. B: Struct. Sci. **B46**, 703 (1990).
[6] K. Hiraga, F. J. Lincoln, and W. Sun, Mater. Trans., JIM **32**, 308 (1991).
[7] K. Edagawa, M. Ichikara, K. Suzuki, and S. Takeuchi, Philos. Mag. Lett. **61**, 19 (1992).
[8] X. Z. Liao, K. H. Kuo, H. Zhang, and K. Urban, Philos. Mag. B **66**, 549 (1992).
[9] W. Steurer, J. Non-Cryst. Solids **153-154**, 92 (1993).
[10] W. Steurer, T. Haibach, B. Zhang, S. Kek, and R. Lück, Acta Crystallogr., Sect. B: Struct. Sci. **B49**, 661 (1993).
[11] W. Steurer, Mater. Sci. Forum **150-151**, 15 (1994).
[12] M. Fettweiss, P. Lanois, F. Denoyer, R. Reich, and M. Lambert,

Phys. Rev. B **49**, 15 573 (1994).
[13] K. Hiraga, W. Sun, and A. Yamamoto, Mater. Trans., JIM **35**, 657 (1994).
[14] K. Tsuda, Y. Nishida, K. Saitoh, M. Tanaka, A. P. Tsai, A. Inoue, and T. Masumoto, Philos. Mag. A **74**, 697 (1996).
[15] W. Steurer, M. Honal, and T. Haibach, in *Proceedings of the 6th International Conference on Quasicrystals, Tokyo, 1997*, edited by S. Takeuchi and T. Fujiwara (World Scientific, Singapore, 1997), p. 355.
[16] S. Ritsch, C. Beeli, H.-U. Nissen, T. Gödecke, M. Scheffer, and R. Lück, Philos. Mag. Lett. **78**, 67 (1998), and references therein.
[17] K. Edagawa, H. Tamaru, S. Yamaguchi, K. Suzuki, and S. Takeuchi, Phys. Rev. B **66**, 12 413 (1994).
[18] B. Grushko, in *Proceedings of Aperiodic 94*, edited by G. Chapuis and W. Paciorek (World Scientific, Singapore, 1995), p. 573.
[19] A. Fujiwara, A. Inoue, and A. P. Tsai, in *Proceedings of the 6th International Conference on Quasicrystals, Tokyo, 1997* (Ref. 15), p. 341.
[20] S. E. Burkov, Phys. Rev. Lett. **67**, 614 (1991).
[21] S. E. Burkov, Phys. Rev. B **47**, 12 325 (1993).
[22] A. Yamamoto and S. Weber, Phys. Rev. Lett. **78**, 4430 (1997).
[23] A. Yamamoto, K. Kato, T. Shibuya, and S. Takeuchi, Phys. Rev. Lett. **65**, 1603 (1990).
[24] C. L. Henley, J. Non-Cryst. Solids **153-154**, 172 (1993).
[25] A. Yamamoto, S. Weber, and A. P. Tsai, in *Proceedings of the 6th International Conference on Quasicrystals, Tokyo, 1997* (Ref. 15), p. 77.
[26] S. Ritsch, C. Beeli, H.-U. Nissen, and R. Lück, Philos. Mag. A **71**, 671 (1995).
[27] D. Joseph, S. Ritsch, and C. Beeli, Phys. Rev. B **55**, 8175 (1997).
[28] F. Frey, K. Hradil, B. Grushko, and G. Y. McIntyre, in *Proceedings of the 6th International Conference on Quasicrystals, Tokyo, 1997* (Ref. 15), p. 379.
[29] S. Ritsch, H.-U. Nissen, and C. Beeli, in *Proceedings of the 5th International Conference on Quasicrystals, Avignon, 1995*, edited by C. Janot and R. Mosseri (World Scientific, Singapore, 1995), p. 216.
[30] L. Shu-yuan, W. Xue-mei, L. Li, Z. Dian-lin, L. X. He, and K. X. Kuo, Phys. Rev. B **41**, 9625 (1990).
[31] S. Martin, A. F. Hebard, A. R. Kortran, and F. A. Thiel, Phys. Rev. Lett. **67**, 719 (1991).
[32] W. Yun-ping and Z. Dian-lin, Phys. Rev. B **49**, 13 204 (1994).
[33] Z. Dian-lin, C. Shao-dum, W. Yun-ping, L. Li, W. Xue-mei, X. L. Ma, and K. H. Kuo, Phys. Rev. Lett. **66**, 2778 (1991).
[34] A. D. Bianchi, E. Felder, M. Kenzelmann, M. A. Chernikov, H. R. Ott, and K. Edagawa, in *Proceedings of the 6th International Conference on Quasicrystals, Tokyo, 1997* (Ref. 15), p. 471.
[35] D. N. Basov, T. Timusk, F. Barakat, J. Greedan, and B. Grushko, Phys. Rev. Lett. **72**, 1937 (1994).
[36] R. Lück and S. Kek, J. Non-Cryst. Solids **153-154**, 329 (1993).
[37] Z. M. Stadnik, G. W. Zhang, A.-P. Tsai, and A. Inoue, Phys. Rev. B **51**, 11 358 (1995).
[38] Z. M. Stadnik, D. Purdie, M. Garnier, Y. Baer, A.-P. Tsai, A. Inoue, K. Edagawa, S. Takeuchi, and K. H. J. Bushow, Phys. Rev. B **55**, 10 938 (1997).
[39] Z. M. Stadnik, D. Purdie, M. Garnier, Y. Baer, A.-P. Tsai, A. Inoue, K. Edagawa, and S. Takeuchi, in *Proceedings of the 6th International Conference on Quasicrystals, Tokyo, 1997* (Ref. 15), p. 563.
[40] E. Belin-Ferré, Z. Dankhazi, V. Fournée, A. Sadoc, C. Berger, H. Müller, and H. Kirchmayr, J. Phys.: Condens. Matter **8**, 6213 (1996).
[41] V. Fournée, Ph.D. thesis, Université Paris 6, 1998.
[42] G. Trambly de Laissardière and T. Fujiwara, Phys. Rev. B **50**, 9843 (1994).
[43] M. Krajčí, J. Hafner, and M. Mihalkovič, Phys. Rev. B **56**, 3072 (1997).
[44] P. Oelhafen, in *Glassy Metals II*, edited by H. Beck and H. J. Güntherodt (Springer, Berlin, 1983), p. 283.
[45] W. Jank, C. Hausleitner, and J. Hafner, Europhys. Lett. **16**, 473 (1991).
[46] C. Hausleitner, M. Tegze, and J. Hafner, J. Phys.: Condens. Matter **4**, 9557 (1992).
[47] J. Grin, U. Burkhardt, M. Ellner, and K. Peters, J. Alloys Compd. **206**, 243 (1994).
[48] P. Villars and L. D. Calvet, *Pearson's Handbook of Crystallographic Data for Intermetallic Phase* (American Society for Metals, Material Park, OH, 1991), Vol. 1.
[49] M. Mihalkovic, H. Elhor, and J.-B. Suck (unpublished).
[50] V. Heine, D. Bullett, R. Haydock, and M. J. Kelly, in *Solid State Physics*, edited by H. Ehrenreich, D. Turnbull, and F. Seitz (Academic Press, New York, 1980), Vol. 35.
[51] O. K. Andersen, D. Jepsen, and M. Šob, in *Electronic Band Structure and its Applications*, edited by M. Youssouff (Springer, Berlin, 1987).
[52] S. K. Bose, S. S. Jaswal, O. K. Andersen, and J. Hafner, Phys. Rev. B **37**, 9955 (1988).
[53] J. Hafner and M. Krajčí, Phys. Rev. B **47**, 1084 (1993); J. Phys.: Condens. Matter **5**, 2489 (1993).
[54] M. U. Lucchini and C. M. M. Nex, J. Phys. C **20**, 3125 (1987).
[55] U. von Barth and L. Hedin, J. Phys. C **4**, 2064 (1972).
[56] T. Rieth and M. Schreiber, J. Phys.: Condens. Matter **10**, 783 (1998).
[57] J. J. Yeh and F. Lindau, At. Data Nucl. Data Tables **32**, 1 (1985).